The Cryosphere Discuss., doi:10.5194/tc-2016-129, 2016
Manuscript under review for journal The Cryosphere
Published: 14 July 2016
© Author(s) 2016. CC-BY 3.0 License.

The Cryosphere
Discussions
Open Access
EGU

Response of seasonal soil freeze depth to climate change across China

Xiaoqing Peng[1,2], Oliver W. Frauenfeld[2], Tingjun Zhang[1*], Kang Wang[3], Bin Cao[1,4], Xinyue Zhong[5], Hang Su[1], Cuicui Mu[1]

[1] Key Laboratory of Western China's Environmental Systems（Ministry of Education), College of Earth and Environmental Sciences, Lanzhou University, Lanzhou, 730000, China

[2] Department of Geography, Texas A&M University, College Station, TX 77843-3147, USA

[3] Institute of Arctic and Apline Research, University of Colorado at Boulder, Boulder, CO 80309, USA

[4] Department of Geography & Environmental Studies, Carleton University, Ottawa, Ontario, Canada

[5] Cold and Arid Regions Environmental and Engineering Research Institute, Chinese Academy of Sciences, Lanzhou 730000, China

* *Correspondence to:* Tingjun Zhang (tjzhang@lzu.edu.cn)

Abstract. The response of seasonal soil freeze depth to climate change has repercussions for the surface energy and water balance, ecosystems, the carbon cycle, and soil nutrient exchange. In this study, we use data from 845 meteorological stations to investigate the response of variations in soil freeze depth to climate change across China. Observations include daily air temperature, daily soil temperatures at various depths, mean monthly gridded air temperature, and Normalized Difference Vegetation Index. Results show that soil freeze depth decreased significantly at a rate of −0.18 cm/year, resulting in a net decrease of 8.05 cm over 1967–2012 across China. On the regional scale, soil freeze depth decreases varied between 0.0 and 0.4 cm/year in most parts of China from 1950 to 2009. Combining climatic and non-climatic factors with soil freeze depth, we

The Cryosphere Discuss., doi:10.5194/tc-2016-129, 2016
Manuscript under review for journal The Cryosphere
Published: 14 July 2016
© Author(s) 2016. CC-BY 3.0 License.

conclude that air temperature increases are responsible for the decrease in soil seasonal freeze depth during this period. Changes in snow depth and vegetation are negatively correlated with soil freeze depth. These results are important for understanding the soil freeze/thaw dynamics and the impacts of soil freeze depth on ecosystem and hydrological process.

1 Introduction

There is a globally averaged warming trend of 0.85°C during 1880-2012 based on multiple land and ocean surface temperature dataset (IPCC, 2014). Given that all of the cryosphere's components are inherently sensitive to air temperature changes on different time scales, cryospheric changes serve as indicators of climate change. Frozen ground is an important component of the cryosphere. Permafrost regions underlay approximately 24% of the exposed land surface of the Northern Hemisphere (Zhang et al, 1999), and seasonally frozen ground regions occupy 57% (Zhang et al., 2003),. China is the country with the third-largest frozen ground extent in the world, with a permafrost area of ~2.20×10^6 km^2, or approximately 23% of its land area, mainly on the Tibetan Plateau; regions with seasonally frozen ground occupy more than 80% of the land area (Zhou et al., 2000). Under warming climate conditions, frozen ground regions are vulnerable to subsidence, especially ice-rich permafrost and relatively warm discontinuous permafrost (Osterkamp et al., 2000; Stendel and Christensen, 2002; Morison et al., 2000). Maximum freeze depth of seasonally frozen ground (SFG) and active layer depth over permafrost play a significant role in cold environments all hydrological, ecological, biological, and pedological activities occur within this layer (Hinzman et al., 1991; Kane et al., 1991; Zhao et al., 2004). Simultaneously, soil freeze depth influences the surface and subsurface hydrological cycle, promotes soil texture changes, and alters the availability of soil nutrients for plant growth.

© Author(s) 2016. CC-BY 3.0 License.

The soil freeze/thaw cycle and soil freeze depth variations affect the decomposition of soil organic matter, and greenhouse gas exchanges between the land surface and the atmosphere (Shiklomanov, 2012; Mu et al., 2015). Thus, seasonal soil freeze depth variability—including the maximum soil freeze depth in SFG and maximum thaw depth in permafrost regions—and climate are closely linked.

Due to global climate warming, significant effort has been devoted to permafrost research, such as permafrost variations on the hemispheric-scale, permafrost temperature changes (Romanovsky et al., 2010; Wu and Zhang, 2008; Guglielmin and Cannone, 2012; Streletskiy et al., 2013; Wu et al., 2015), permafrost degradation (Jorgenson et al., 2006; Sannel and Kuhry, 2011; Ravanel et al., 2010; Streletskiy et al., 2015; Park et al., 2016), hydrological processes in permafrost regions (Wang et al., 2009; Hu et al., 2009; Streletskiy et al., 2015; Park et al., 2013; Ford and Frauenfeld, 2016), feedbacks to climate change (Schuur et al., 2008; Park et al., 2015), and other aspects. The increasing thickness of the active layer has been indicated by many observations in permafrost regions at high latitudes (Brown et al., 2000; Frauenfeld et al., 2004; IPCC, 2014; Callaghan et al., 2011; Fyodorov-Davydov et al., 2008; Smith et al., 2010; Wu and Zhang, 2010; Zhang et al, 2005; Zhao et al., 2010; Li et al., 2012; Liu et al., 2014). Less research has focused on SFG areas (Zhang et al., 2003; Frauenfeld et al., 2004; Frauenfeld and Zhang, 2011; Wang et al, 2015), although the near-surface soil freeze/thaw status has been investigated using satellite passive microwave remote sensing (Zhang and Armstrong, 2001; Zhang et al., 2003, 2004; Li et al., 2008; Jin et al., 2015).

Shiklomanov (2012) has similarly pointed out that SFG did not receive much attention despite its vast area extent and importance, mainly due to a lack of long-term observational time

The Cryosphere Discuss., doi:10.5194/tc-2016-129, 2016
Manuscript under review for journal The Cryosphere
Published: 14 July 2016
© Author(s) 2016. CC-BY 3.0 License.

series to document changes. Evaluating climatic and non-climatic changes on SFG requires comprehensive spatial assessments of available soil temperature records (Shiklomanov, 2012). To date, no comprehensive investigation of soil freeze depth in relation to climate change has been conducted in China, despite the prevalence of SFG in this part of the world. Therefore, using long-term observational data, the goals and unique contributions of this study are 1) to estimate China's spatial and temporal variations of seasonal soil freeze depth; 2) to quantify the potential forcing factors of soil freeze depth including climatic and non-climatic factors; and 3) to establish how soil freeze depth variability responds to climate change in China.

2 Data and methods

2.1 Data

2.1.1 Mean daily air and ground surface temperature

Mean daily air temperature and ground surface temperature data are collected from the China Meteorological Administration (CMA) for a total of 839 meteorological stations (Figure 1) available four times daily at 02:00, 08:00, 14:00, and 20:00. These data come already quality controlled, and stations date back to the 1950s and 1960s. Some stations end during the 1990s, while others are available until 2013. Most stations are located in east central China, with fewer sites in the west and at high elevations, such as on the Qinghai-Tibetan Plateau (Figure 1). These mean daily air and ground surface temperatures are used to estimate climate change and to calculate the freeze/thaw index.

2.1.2 Soil temperature

Daily soil temperature data are available for 845 sites across China (Figure 1) from the CMA, and measured at the depths of 0.00, 0.05, 0.1, 0.15, 0.2, 0.4, 0.5, 0.8, 1.6, and 3.2 m. The

The Cryosphere Discuss., doi:10.5194/tc-2016-129, 2016
Manuscript under review for journal The Cryosphere
Published: 14 July 2016
© Author(s) 2016. CC-BY 3.0 License.

record of available soil temperature data varies for these stations, with some observations dating back to the late 1950s, and some only to the 1970s. Some station records end in the 1990s, while others are available through 2006 (Wang et al., 2015). Soil temperature is used to calculate the soil freeze depth; we combine the potential maximum soil seasonal freeze depth in permafrost regions, and maximum soil freeze depth in seasonally frozen ground regions. The number of stations with both daily air temperature and soil temperature observations is 729.

2.1.3 Mean monthly gridded air temperature

Gridded air temperature was used to analyze soil freeze depth at the regional scale across China. We obtained mean monthly gridded air temperature (MMGAT) from the University of Delaware's 1900–2014 terrestrial air temperature gridded monthly time series (http://climate.geog.udel.edu/~climate/), with 0.5°×0.5° spatial resolution. This dataset was produced by combining many observational station records across the world, using spatial interpolation and cross-validation procedures (Legates et al., 1990; Peterson et al., 1997 & 1998; Willmott et al., 1995). The period 1950–2010 is chosen for MMGAT, for assessing its correspondence with the seasonal freeze depth across China.

2.1.4 Digital elevation model (DEM)

We use a DEM from the global 30 arc-second elevation data set (GTOPO30, https://lta.cr.usgs.gov/GTOPO30, Figure 1). The DEM data are used for spatial regridding, as detailed below in section 2.2.

2.1.5 Snow depth

We obtained daily mean snow depth data for 672 sites across China. The period of record at these locations varies, with some stations dating back to the late 1950s and some only to the

The Cryosphere Discuss., doi:10.5194/tc-2016-129, 2016
Manuscript under review for journal The Cryosphere
Published: 14 July 2016
© Author(s) 2016. CC-BY 3.0 License.

1970s. Some station records end around the 1990s while others are available through 2005. These data were used to assess the influence of seasonal snow cover on soil freeze depth.

2.1.6 Normalized differential vegetation index

The NDVI dataset used in this study is from the Global Inventory Modeling and Mapping Studies (GIMMS) team, available for 1982–2006. NDVI is derived from NOAA AVHRR data, available at 15-day temporal resolution, and an 8-km spatial resolution. (Tourre et al., 2008).

2.2 Methods

Daily missing air temperatures are filled in based on highly correlated neighboring sites using linear least squares regression. Similarly, daily missing mean ground surface temperatures are estimated using linear regression with the daily mean air temperature. Based on the daily air temperature and ground surface temperature in each site, we can calculate the mean annual air temperature (MAAT) and mean annual ground surface temperature (MAGST) at each site, respectively.

To improve the original 0.5°×0.5° MMGAT data to a 1-km resolution, spatial interpolation was used in conjunction with the 1-km resolution DEM (e.g., Willmott and Matsuura, 1995; Gruber et al., 2012). The data processing steps are to (1) calculate the average monthly atmospheric lapse rate based on all available meteorological stations across China and their elevations; (2) bring each average monthly gridded air temperature value to sea level using the average monthly lapse rate; (3) apply a Kriging interpolation to the sea-level adjusted MMGAT; (4) bring the gridded sea-level air temperature back to the DEM-gridded height. Based on more than 800 sites, we test the interpolated MMGAT and observational monthly air temperature, and find that the regression coefficient is almost 1.0 with a minimum of 0.98 in April.

© Author(s) 2016. CC-BY 3.0 License.

The freezing/thawing index can also be an important indicator to assess the variations in frozen ground (Zhang et al, 1997; Frauenfeld et al., 2007; Nelson, 2003). In general, there are two types of freezing/thawing indices: the surface freezing/thawing index, calculated from ground surface temperature, and the air freezing/thawing index, computed from air temperature. Daily mean air temperature and ground surface temperature at 839 meteorological stations were used to obtain both variants of the freezing/thawing index. For the regional-scale air freezing/thawing index, we employ the methodology of Zhang et al. (1997) and Frauenfeld et al. (2007), and the methodology of Peng et al. (2013) for the adjusted 1-km gridded terrestrial air temperature data.

We calculate the annual maximum snow depth (SND) from the daily data for 1 July–30 June, and match up those snow depth stations with the soil temperature stations. If there is missing data in the spring, autumn and winter season of one station, this station data will not be used.

Various methods are available to calculate the soil freeze depth. For example, it can be estimated directly from soil temperature, from physical and statistical models, and based on the Stefan solution. In this study, we use the Stefan solution to estimate soil freeze depth, which is determined using equation 1:

$$\mathrm{SFD} = \sqrt{2K_f\left(\frac{n_f FI_a}{P_b w L}\right)} \quad (1)$$

where SFD is soil freeze depth (m), K_f is the thermal conductivity of the frozen soil (W/mºC), n_f is the n-factor for the freezing season and corresponds to the ratio between the surface freezing index and the air freezing index (Peng et al., 2016), FI_a is the annual air freezing index (ºC•d), P_b is the soil bulk density (kg/m^3), w the soil water content by weight, and L the latent heat of fusion (J/kg) (Zhang et al., 2005). In equation 1, many site-specific factors are required to estimate SFD, which are not easily obtained, particularly at the regional scale. Based on the SFD and annual

The Cryosphere Discuss., doi:10.5194/tc-2016-129, 2016
Manuscript under review for journal The Cryosphere
Published: 14 July 2016
© Author(s) 2016. CC-BY 3.0 License.

freezing index at observational sites, however, we can quantify the relationship between these two parameters (Figure 2) and find a strong and statistically significant correlation of R=0.87. Thus, the relationship between SFD and the annual freezing index can be simplified (Harlan and Nixon, 1978) as:

$$\mathrm{SFD} = \mathrm{E}\sqrt{\mathrm{FI_a}} \quad (2)$$

Where E is defined (Nelson and Outcalt, 1987) as:

$$\mathrm{E} = \sqrt{\frac{2\mathrm{K_f n_f}}{\mathrm{P_b wL}}} \quad (3)$$

To estimate the SFD at the regional scale across China, we first calculate SFD for every observational station by interpolating the depth of the 0°C isotherm throughout the 0.0～3.2 m temperature profile using the daily mean soil temperature (Frauenfeld et al., 2004). Next, we estimate the FI_a based on the calculations in Frauenfeld et al. (2007). To estimate the E value for all stations we use the SFD, FI_a, and equations 2 and 3. Then, we interpolate the E value to the regional scale at 1-km resolution using kriging in ArcGIS. The SFD is estimated across China based on equation 2, the 1-km E value, and FI_a. We can then estimate the regional-scale SFD for each year from 1950 to 2009 across China, and obtain the mean decadal SFD. Finally, using regression analysis, we estimate the SFD trend at the regional scale across China.

From the 1-km scale E factor values, we can extract every site's E factor based on the sites' latitude and longitude. Then, the air freezing index from the sites is used to calculate the annual soil freeze depth at every site by equation 2. To verify the accuracy, we compare the observational SFD calculated from the soil temperature, and the simulated SFD calculated by the Stefan method (Figure 3). The result demonstrates that the mean absolute error and root-mean-square error are 0.08 m and 0.14 m, respectively. It shows that there is a good

The Cryosphere Discuss., doi:10.5194/tc-2016-129, 2016
Manuscript under review for journal The Cryosphere
Published: 14 July 2016
© Author(s) 2016. CC-BY 3.0 License.

agreement between simulated and observational SFD by this method. To find the potential forcing variables of the observed long-term SFD changes across China, a number of factors are related to SFD: MAAT, MAGST, freezing index, thawing index, SND, and NDVI. We used correlation to analyze the relationship between these variables with SFD, and employ a 95%-significance level for all statistical analyses.

3 Results

3.1 Soil freeze depth

Based on every site's E factor and FI_a, we calculate the spatial variability and trends of SFD at every location (Figure 4). The highest SFD was mainly located in northeastern and northwestern China, and the Tibetan Plateau. In contrast, the lowest SFD was found in the south of China. Locations with SFD greater than 0.4 m are found north of the Yellow River. In the northwest of China, locations with SFD less than 0.8 m are found in the Taklamakan desert, and some sites with SFD greater than 2.0 m are located in the Altai, Tianshan, and Pamir Mountains. There are several possible reasons for these observed SFD differences in the northwest of China. In the desert, the mean annual air temperature is higher and the elevation is lower than in the surrounding Altai, Tianshan, and Pamir Mountains. Precipitation in the desert is lower, which can affect the soil moisture and the soil thermal conductivity, such that low soil moisture is related to low thermal conductivity. Vegetation cover can also influence the albedo and temperature, affecting the SFD. The albedo in the desert is larger than the vegetated regions, which can affect the net solar radiation, resulting the shallower SFD in desert regions. Combined, these possible factors can account for the spatial differences in SFD in the northwest of China.

On the Tibetan Plateau, most sites have a SFD greater than 2.4 m. There is an increase in

The Cryosphere Discuss., doi:10.5194/tc-2016-129, 2016
Manuscript under review for journal The Cryosphere
Published: 14 July 2016
© Author(s) 2016. CC-BY 3.0 License.

SFD with increasing latitude and elevation. The significant magnitude of SFD change is between -0. 4 and less than 0 cm/year. The sites with the strongest decreasing trends of -1.2 cm/year are on Tibetan Plateau and -1.0 cm/year in the north of China.

Based on the sites' E factors and FI_a, we calculate SFD time series anomalies from 1951 to 2012 (Figure 5). Although a composite time series of all available stations data can be calculated during 1951–2012, few of the 839 stations actually contribute to the mean values before the 1960s (Figure 5). There are fewer than 200 stations in the early years, and therefore does not represent the SFD across China as a whole. Beginning in 1967 more than 800 stations contribute to each year's mean, therefore long-term SFD trends will only be evaluated from then on. There is a statistically significant change in SFD anomalies of -0.18 cm/year, corresponding to a net decrease of 8.05 cm. In addition to the overall long-term decrease, there are also some patterns of inter-decadal variability during 1967-2012, including slight positive changes in some periods. SFD exhibited both increases and decreases until 1975, followed by a sharp decrease until 1990. However, SFD has remained constant or may perhaps be increasing slightly during 1990-2012. Therefore, the overall SFD change during 1967–2012 was largely controlled by the decrease during 1975–1990 period. Similar SFD changes, attributable to the North Atlantic Oscillation, were found in high-latitude Eurasia (Frauenfeld and Zhang, 2011).

3.2 Spatial and temporal variability of SFD in China

Based on the 1-km resolution E factor and 1-km FI_a calculated from MMGAT, we estimate SFD across China from 1950 to 2009 by the Stefan method. Figure 6 shows the spatial variability of mean decadal SFD. The overall spatial pattern of SFD variability is quite consistent. Thus, we describe the spatial pattern of SFD from the 1950s as an example. SFD increases with

© Author(s) 2016. CC-BY 3.0 License.

latitude and elevation, with SFD greater than 1.5 m in northeastern China, the Mongolia Plateau, Tibetan Plateau, and north of the Xinjiang region. In the east of China, the SFD ranges from 0.0 m to more than 4.0 m, and increases with latitude. In the Yellow River region, the elevation decreases from west to east, while the SFD varies from greater than 2.5 m to less than 0.5 m. The SFD in the Taklimakan desert is lower than in the surrounding area.

Figure 7 represents the SFD trend across China from 1950 to 2009. The gray region represents areas where the SFD trends are not statistically significant, however, they are statistically significant in all other regions. In general, the SFD decreased significantly over northern China, except in two small areas. The SFD trend ranges between 0.0 and -0.4 cm/year in most areas. SFD trends less than -0.4 cm/year are found in some areas, such as the Tibetan Plateau, and the Pamirs. In the two small areas of increasing SFD, we further investigated the MAAT trend during 1950-2010 based on the MMGAT dataset. There is similarly a statistically significant decrease of MAAT in these same areas during this period. Thus, air temperature is one of the important factors that influences the soil freeze depth in these areas.

Overall, the spatial variability indicates that SFD changes with latitude and elevation at the regional scale across China. As is expected from climate warming, a statistically significant decreasing trend in SFD is evident across China from 1950 to 2009.

3.3 Potential forcing variables

To explore the possible variables leading to the documented changes in SFD, we analyze potentially important factors for soil freeze dynamics: MAAT, MAGST, freezing index including FI_a and the ground surface freezing index (FI_s), thawing index including the air (TI_a) and ground surface thawing index (TI_s), SND, and NDVI. Temperature—including MAGST and MAAT—at

© Author(s) 2016. CC-BY 3.0 License.

the 839 station locations exhibits a statistically significant increase over the 1951–2013 period of 0.019 and 0.013 °C/year, or approximately 1.2 °C and 0.78 °C over the 63 years, respectively (Figure 8 a, and b). MAGST and MAAT are statistically significantly correlated with SFD at R=-0.56 and R=-0.66, which means that 31% and 44% of the variability in SFD can be accounted for by these temperature measures. Further, the negative correlation demonstrates that increasing temperatures result in SFD decreases at the 839 stations.

Soil freeze usually begins in autumn or winter, with temperatures less than 0°C, reaching their maximum freeze depth toward the end of winter season or spring. Therefore, maximum annual SFD occurs during the cold seasons. Freezing index is thus an important indicator for accumulated cold season temperatures (Frauenfeld and Zhang, 2011). From 1951 to 2013, FI_s and FI_a underwent a statistically significant decrease of 3.0 and 1.62 °C-days/year, respectively (Figure 8 c, and d), indicating warming, which reduces the cold season's magnitude and/or duration. The correlation between FI_s, FI_a, and SFD was a statistically significant 0.68 and 0.87, indicating that the FI accounts for 46% and 76% of SFD variability.

The thawing index is used to assess the accumulated positive degree-days during the warm season (Frauenfeld and Zhang, 2011). There are no obvious TI changes at the station locations until approximately 1985. The TI increases during 1985-2008, followed by a decrease until 2013. From 1951 to 2013, TI_s and TI_a show statistically significant increases at a magnitude of 3.73 and 2.77 °C-days/year, respectively (Figure 8 e and f). The correlation coefficient between TI_s, TI_a, and SFD is -0.53 and -0.57, respectively, indicating a weak negative association such that warm summer conditions correspond to a shallower SFD the following cold season.

Figure 9 shows the correlation between SFD and SND. There was no statistically

The Cryosphere Discuss., doi:10.5194/tc-2016-129, 2016
Manuscript under review for journal The Cryosphere
Published: 14 July 2016
© Author(s) 2016. CC-BY 3.0 License.

significant trend in SND for the 1951–2005 period. Also, SND is not statistically significantly correlated with SFD (Figure 9).

As suggested by Shiklomanov (2012), non-climatic factors likely also affect SFD. The surface can be affected directly by climate forcing, while the subsurface effects are more complex. The subsurface soil only indirectly receives a climatic signal, which is furthermore altered by site-specific soil processes (e.g., thermal conductivity and analogous soil properties). Vegetation is a likely non-climatic factor that influences the soil freeze depth (Shiklomanov, 2012). Thus, we investigate vegetation using NDVI (Peng et al., 2013) and find it is significantly correlated with SFD at -0.80, suggesting that 64% of the variability in SFD can be accounted for by NDVI. The statistically significant negative correlation demonstrates that when NDVI increases (more greening), this corresponds to a decrease in SFD (Figure 10).

4 Discussion

Soil freeze-thaw changes involve a series of processes, such as energy exchanges, soil moisture exchanges, and gases exchanges between the atmospheric and terrestrial system. Therefore, variations of soil freeze/thaw most likely have an important effect on geomorphic, hydrological, and biological processes. As freeze/thaw depth changes, these variations may have destabilizing effects on engineering structures, such as on improperly constructed infrastructure (Smith and Burgess, 1999; Stendel and Christensen, 2002). The release of additional amounts of greenhouse gases to the atmosphere also occurs (Michaelson et al., 1996; Mu et al., 2015). In this paper, we use the Stefan method to calculate SFD, analyze the spatial SFD variability and trends, and quantify the potential driving factors affecting SFD.

4.1 Climatic and non-climatic factors

© Author(s) 2016. CC-BY 3.0 License.

SFD changes can influence the environmental and natural systems, and are also affected by variables such as air temperature, ground surface temperature, freezing/thawing index, and vegetation. SFD is vulnerable to climate warming. Many examples of permafrost degradation have been reported, such as deeper the active layer thickness, reduced freeze time duration, and shifts in the timing of thawing and freezing in seasonally frozen ground regions (Wang et al., 2015; Callaghan et al., 2011; IPCC, 2014; Henry 2008). Negative correlations are found here between SFD and temperature (including MAAT and MAGST), because of solar radiation heating the ground, energy transfer into the soil, ultimately increasing the soil temperature. Thus, increasing temperature is found to be the main factor influencing SFD variability in China, as in previous work focusing only on the Tibetan Plateau (Zhao et al., 2004).

The freezing/thawing indices represent the accumulated negative and positive degree days in the cold and warm seasons, respectively (Wu et al., 2011). The positive and negative correlation between SFD and FI and TI were statistically significant, consistent with previous results in other regions (Frauenfeld and Zhang, 2011). Due to the maximum soil freeze depth occurring in the cold season and SFD being affected by temperature, the positive correlation between SFD and FI is reasonable. Although TI is the accumulated temperature in the warm season, it takes some time to transfer the energy into the deeper ground. The energy flux into the soil reduces with increasing soil depth. Therefore, if all the conditions are the same, a larger TI can precondition the ground by increasing the energy in the deeper soil, which can subsequently delay soil freezing. Thus, the TI can indirectly influence soil temperature to some extent (Frauenfeld and Zhang, 2011).

Snow depth can have an effect on soil temperature, which would affect the active layer thickness and soil seasonal freeze depth variability. Numerical modeling studies have shown that

The Cryosphere Discuss., doi:10.5194/tc-2016-129, 2016
Manuscript under review for journal The Cryosphere
Published: 14 July 2016
© Author(s) 2016. CC-BY 3.0 License.

snow depth does impact SFD (Zhang and Stamnes, 1998; Ling and Zhang, 2003; Park et al., 2015). Park et al. (2015) indicated that both increasing SND and snow structure changes were favorable to soil warming, resulting in active layer thickness decreasing in northern regions as previously found by Frauenfeld et al. (2004). Snow cover insulates the ground during the cold season (Zhang, 2005). Interestingly, in our study we did not find a relationship between SND and SFD. This could be due to the spatial heterogeneity of snow across China. According previous research, the snow depth, snow water equivalent, and snow densities are smallest on the Tibetan Plateau compared to other parts of China (Ma et al., 2012). Compared with other regions, multi-year average snow depth in general is low in China, especially on the Tibetan Plateau and the east-central mountain regions of China (Zhong et al., 2014), and may therefore have only limited insulating effects. This could lead to the lack of a relationship between SFD and SND across China and motivates further future investigation.

A negative correlation between SFD and vegetation, as quantified by NDVI, is found. Vegetation change has a significant influence on the climate system mostly through changes to the surface radiative energy budget, which can be affected the SFD. Based on previous research, vegetation varies in different land cover types and responds to climate change via different physical mechanisms (Snyder et al., 2004). These involve, in general, changes in the surface albedo (e.g., bare ground versus vegetation cover), the variability of cloud cover which strongly influences the radiative balance at the surface, the roughness of the surface, vegetation transpiration, and shading effects (Kelley et al., 2004; Chang et al., 2012; Zhang et al., 2012; Snyder et al., 2004; Swann et al., 2010). Compared to no vegetation cover, vegetation causes a large annual-average increase in the surface albedo with the largest changes in the winter and

The Cryosphere Discuss., doi:10.5194/tc-2016-129, 2016
Manuscript under review for journal The Cryosphere
Published: 14 July 2016
© Author(s) 2016. CC-BY 3.0 License.

spring seasons, which reduces the amount of net radiation absorbed at the surface, making the surface colder. Removal of vegetation cover reduces the roughness of the surface and increases the low-level winds, resulting in enhanced advection. Furthermore, reducing vegetation cover can lead to increases in low-level cloud cover, resulting in reduced incoming shortwave radiation, and keeping the surface colder (Snyder et al., 2004). While we observe a negative correlation between vegetation and SFD, the detailed physical mechanism will require further future work.

5 Summary and Conclusions

In this study, we conducted a comprehensive regional-scale investigation of SFD over China. As a significant climate indicator, SFD is influenced by many variables including climatic and non-climatic factors. These factors are often integrated to affect SFD (Lachenbruch and Marshall, 1986; Brown et al., 2000; Frauenfeld et al., 2004). Our results can be summarized as follows:

The spatial distribution of SFD variability is influenced by latitude and elevation across China. High latitude and altitude sites are characterized by high SFD. In contrast, lower SFD values are mainly observed for lower latitude and lower elevation regions.

Of the total 839 sites, we find that the SFD decreased significantly, at -0.18 cm/year from 1967 to 2012, equal to a net change of 8.05 cm. The long-term decrease also indicated inter-decadal variability, including some positive changes in some periods and no change since 1990.

On the regional scale, the 1950–2009 spatial variation of SFD ranges between 0.0 and 4.5 m across China, with most areas exhibiting significant decreases between less than 0.0 and -0.4 cm/year. Climatic and non-climatic factors as potential driving variables for SFD were

© Author(s) 2016. CC-BY 3.0 License.

explored. A negative relationship is evident between SFD and MAAT, MAGST, TI_a, and TI_s, with statistically significant correlations of -0.66, -0.56, -0.57, and -0.56, respectively. The climatic factors FI_s and FI_a were correlated positively with SFD, at 0.87 and 0.68, respectively. There is no correlation between SFD and SND. The non-climatic factor vegetation (NDVI) is negatively correlated with SFD, indicating that 64% of the changes in SFD can be accounted for by vegetation.

Acknowledgments: This study was funded by the National Natural Science Foundation of China (grant No. 91325202), the National Key Scientific Research Program of China (grant No. 2013CBA01802), and the Fundamental Research Funds for the Central Universities (lzujbky-2015-217). The land cover data were obtained from the Environmental and Ecological Science Data Center for West China (http://westdc.westgis.ac.cn/). We acknowledge computing resources and time at the Supercomputing Center of Cold and Arid Region Environment and Engineering Research Institute of Chinese Academy of Sciences.

References

Brown, J., Hinkel, K., and Nelson, F.: The circumpolar active layer monitoring (calm) program: Research designs and initial results 1, Polar geography, 24, 166-258, 2000.

Callaghan, T. V., Tweedie, C. E., and Webber, P. J.: Multi-decadal changes in tundra environments and ecosystems: the International Polar Year-Back to the Future Project (IPY-BTF), Ambio, 40, 555-557, 2011.

Christiansen, H. H., Etzelmüller, B., Isaksen, K., Juliussen, H., Farbrot, H., Humlum, O., Johansson, M., Ingeman-Nielsen, T., Kristensen, L., and Hjort, J.: The thermal state of permafrost in the Nordic area during the International Polar Year 2007–2009, Permafrost and Periglacial Processes, 21, 156-181, 2010.

Ford, T. W. and Frauenfeld, O. W.: Surface–Atmosphere Moisture Interactions in the Frozen Ground Regions of Eurasia, Scientific reports, 6, 19163, 2016.

Frauenfeld, O. W. and Zhang, T.: An observational 71-year history of seasonally frozen ground changes in the Eurasian high latitudes, Environmental Research Letters, 6, 044024, 2011.

Frauenfeld, O. W., Zhang, T., Barry, R. G., and Gilichinsky, D.: Interdecadal changes in seasonal freeze and thaw depths in Russia, Journal of Geophysical Research: Atmospheres, 109, 2004.

Frauenfeld, O. W., Zhang, T., and Mccreight, J. L.: Northern hemisphere freezing/thawing index

© Author(s) 2016. CC-BY 3.0 License.

variations over the twentieth century, International Journal of Climatology, 27, 47-63, 2007.

Fyodorov-Davydov, D., Kholodov, A., Ostroumov, V., Kraev, G., Sorokovikov, V., Davudov, S., and Merekalova, A.: Seasonal thaw of soils in the North Yakutian ecosystems, 2008, 481-486.

Gruber, S.: Derivation and analysis of a high-resolution estimate of global permafrost zonation, Cryosphere, 6, 221-233, 2012.

Guglielmin, M. and Cannone, N.: A permafrost warming in a cooling Antarctica?, Climatic Change, 111, 177-195, 2012.

Harlan, R. and Nixon, J.: Ground thermal regime, Geotechnical engineering for cold regions, 1978. 103-163, 1978.

Henry, H. A.: Climate change and soil freezing dynamics: historical trends and projected changes, Climatic Change, 87, 421-434, 2008.

Hinzman, L., Kane, D., Gieck, R., and Everett, K.: Hydrologic and thermal properties of the active layer in the Alaskan Arctic, Cold Regions Science and Technology, 19, 95-110, 1991.

Hu, H., Wang, G., Wang, Y., Liu, G., Li, T., and Ren, D.: Response of soil heat-water processes to vegetation cover on the typical permafrost and seasonally frozen soil in the headwaters of the Yangtze and Yellow Rivers, Chinese Science Bulletin, 54, 1225-1233, 2009.

Intergovernmental Panel on Climate Change: Climate Change 2014–Impacts, Adaptation and Vulnerability: Regional Aspects, Cambridge University Press, 2014.

Jin, R., Zhang, T., Li, X., Yang, X., and Ran, Y.: Mapping surface soil freeze-thaw cycles in China based on SMMR and SSM/I brightness temperatures from 1978 to 2008, Arctic, Antarctic, and Alpine Research, 47, 213-229, 2015.

Jorgenson, M. T., Shur, Y. L., and Pullman, E. R.: Abrupt increase in permafrost degradation in Arctic Alaska, Geophysical Research Letters, 33, 2006.

Kane, D. L., Hinzman, L. D., and Zarling, J. P.: Thermal response of the active layer to climatic warming in a permafrost environment, Cold Regions Science and Technology, 19, 111-122, 1991.

Kelley, A. M., Epstein, H. E., and Walker, D. A.: Role of vegetation and climate in permafrost active layer depth in arctic tundra of northern Alaska and Canada, Journal of Glaciology and Geocryology, 26, 269-274, 2004.

Lachenbruch, A. H. and Marshall, B. V.: Changing climate: geothermal evidence from permafrost in the Alaskan Arctic, Science, 234, 689-696, 1986.

Legates, D. R. and Willmott, C. J.: Mean seasonal and spatial variability in gauge-corrected, global precipitation, International Journal of Climatology, 10, 111-127, 1990.

Li, R., Zhao, L., Ding, Y., Wu, T., Xiao, Y., Du, E., Liu, G., and Qiao, Y.: Temporal and spatial variations of the active layer along the Qinghai-Tibet Highway in a permafrost region, Chinese Science Bulletin, 57, 4609-4616, 2012a.

Li, X., Cheng, G., Jin, H., Kang, E., Che, T., Jin, R., Wu, L., Nan, Z., Wang, J., and Shen, Y.: Cryospheric change in China, Global and Planetary Change, 62, 210-218, 2008.

Li, X., Jin, R., Pan, X., Zhang, T., and Guo, J.: Changes in the near-surface soil freeze–thaw cycle on the Qinghai-Tibetan Plateau, International Journal of Applied Earth Observation and Geoinformation, 17, 33-42, 2012b.

Ling, F. and Zhang, T.: Numerical simulation of permafrost thermal regime and talik development under shallow thaw lakes on the Alaskan Arctic Coastal Plain, Journal of Geophysical Research: Atmospheres, 108, 2003.

Liu, L., Jafarov, E. E., Schaefer, K. M., Jones, B. M., Zebker, H. A., Williams, C. A., Rogan, J.,

© Author(s) 2016. CC-BY 3.0 License.

and Zhang, T.: InSAR detects increase in surface subsidence caused by an Arctic tundra fire, Geophysical Research Letters, 41, 3906-3913, 2014a.

Liu, L., Schaefer, K., Gusmeroli, A., Grosse, G., Jones, B. M., Zhang, T., Parsekian, A. D., and Zebker, H. A.: Seasonal thaw settlement at drained thermokarst lake basins, Arctic Alaska, Atmospheric Chemistry and Physics, 8, 815, 2014b.

M, C. X. L. J. H. J. W. Y. P. Z. Y. L. Z. G. Y. C. F. Q. Z. Y.: Influences of vegetation on permafrost: a review, Acta Ecologica Sinica, 32, 7981-7990, 2012.

Ma, L.-J. and Qin, D.-H.: Spatial-Temporal Characteristics of Observed Key Parameters for Snow Cover in China during 1957--2009, Journal of Glaciology and Geocryology, 34, 1-11, 2012.

Michaelson, G. J., Ping, C., and Kimble, J.: Carbon storage and distribution in tundra soils of Arctic Alaska, USA, Arctic and Alpine Research, 1996. 414-424, 1996.

Morison, J., Aagaard, K., and Steele, M.: Recent environmental changes in the Arctic: a review, Arctic, 2000. 359-371, 2000.

Mu, C., Zhang, T., Wu, Q., Cao, B., Zhang, X., Peng, X., Wan, X., Zheng, L., Wang, Q., and Cheng, G.: Carbon and nitrogen properties of permafrost over the Eboling Mountain in the upper reach of Heihe River basin, Northwestern China, Arctic, Antarctic, and Alpine Research, 47, 203-211, 2015.

Nelson, F. E.: (Un) frozen in time, Science, 299, 1673, 2003.

Nelson, F. E. and Outcalt, S. I.: A computational method for prediction and regionalization of permafrost, Arctic and Alpine Research, 1987. 279-288, 1987.

Osterkamp, T., Viereck, L., Shur, Y., Jorgenson, M., Racine, C., Doyle, A., and Boone, R.: Observations of thermokarst and its impact on boreal forests in Alaska, USA, Arctic, Antarctic, and Alpine Research, 2000. 303-315, 2000.

Park, H., Fedorov, A. N., Zheleznyak, M. N., Konstantinov, P. Y., and Walsh, J. E.: Effect of snow cover on pan-Arctic permafrost thermal regimes, Climate Dynamics, 44, 2873-2895, 2015.

Park, H., Kim, Y., and Kimball, J. S.: Widespread permafrost vulnerability and soil active layer increases over the high northern latitudes inferred from satellite remote sensing and process model assessments, Remote Sensing of Environment, 2016. 2016.

Park, H., Walsh, J., Fedorov, A., Sherstiukov, A., Iijima, Y., and Ohata, T.: The influence of climate and hydrological variables on opposite anomaly in active-layer thickness between Eurasian and North American watersheds, The Cryosphere, 7, 631-645, 2013.

Peng, X., Zhang, T., Cao, B., Wang, Q., Wang, K., Shao, W., and Guo, H.: Changes in freezing-thawing index and soil freeze depth over the Heihe River Basin, western China, Arctic, Antarctic, and Alpine Research, 48, 161-176, 2016.

Peng, X., Zhang, T., Zhong, X., Wang, Q., and Wang, K.: Spatial and temporal variations of NDVI and its response to meteological factors over Heihe River Basin of Qilian Mountains, Journal of Lanzhou University (Natural Sciences), 2013. 192-202, 2013.

Peterson, T. C., Vose, R., Schmoyer, R., and Razuvaëv, V.: Global Historical Climatology Network (GHCN) quality control of monthly temperature data, International Journal of Climatology, 18, 1169-1179, 1998.

Peterson, T. C. and Vose, R. S.: An overview of the Global Historical Climatology Network temperature database, Bulletin of the American Meteorological Society, 78, 2837-2849, 1997.

Ravanel, L., Allignol, F., Deline, P., Gruber, S., and Ravello, M.: Rock falls in the Mont Blanc Massif in 2007 and 2008, Landslides, 7, 493-501, 2010.

The Cryosphere Discuss., doi:10.5194/tc-2016-129, 2016
Manuscript under review for journal The Cryosphere
Published: 14 July 2016
© Author(s) 2016. CC-BY 3.0 License.

Romanovsky, V. E., Smith, S. L., and Christiansen, H. H.: Permafrost thermal state in the polar Northern Hemisphere during the international polar year 2007–2009: a synthesis, Permafrost and Periglacial Processes, 21, 106-116, 2010.

Sannel, A. and Kuhry, P.: Warming-induced destabilization of peat plateau/thermokarst lake complexes, Journal of Geophysical Research: Biogeosciences, 116, 2011.

Schuur, E. A., Bockheim, J., Canadell, J. G., Euskirchen, E., Field, C. B., Goryachkin, S. V., Hagemann, S., Kuhry, P., Lafleur, P. M., and Lee, H.: Vulnerability of permafrost carbon to climate change: implications for the global carbon cycle, BioScience, 58, 701-714, 2008.

Shiklomanov, N. and Nelson, F.: Active-layer mapping at regional scales: A 13-year spatial time series for the Kuparuk region, north-central Alaska, Permafrost and Periglacial Processes, 13, 219-230, 2002.

Shiklomanov, N. I.: Non-climatic factors and long-term, continental-scale changes in seasonally frozen ground, Environmental Research Letters, 7, 011003, 2012.

Smith, S., Romanovsky, V., Lewkowicz, A., Burn, C., Allard, M., Clow, G., Yoshikawa, K., and Throop, J.: Thermal state of permafrost in North America: a contribution to the international polar year, Permafrost and Periglacial Processes, 21, 117-135, 2010.

Smith, S. L. and Burgess, M. M.: Mapping the sensitivity of Canadian permafrost to climate warming, IAHS PUBLICATION, 1999. 71-80, 1999.

Snyder, P., Delire, C., and Foley, J.: Evaluating the influence of different vegetation biomes on the global climate, Climate Dynamics, 23, 279-302, 2004.

Stendel, M. and Christensen, J.: Impact of global warming on permafrost conditions in a coupled GCM, Geophysical Research Letters, 29, 2002.

Streletskiy, D., Anisimov, O., Vasiliev, A., and Whiteman, C.: Permafrost degradation, Snow and Ice-Related Hazards, Risks, and Disasters, 2014. 303, 2014.

Streletskiy, D. A., Sherstiukov, A. B., Frauenfeld, O. W., and Nelson, F. E.: Changes in the 1963–2013 shallow ground thermal regime in Russian permafrost regions, Environmental Research Letters, 10, 125005, 2015a.

Streletskiy, D. A., Tananaev, N. I., Opel, T., Shiklomanov, N. I., Nyland, K. E., Streletskaya, I. D., and Shiklomanov, A. I.: Permafrost hydrology in changing climatic conditions: seasonal variability of stable isotope composition in rivers in discontinuous permafrost, Environmental Research Letters, 10, 095003, 2015b.

Swann, A. L., Fung, I. Y., Levis, S., Bonan, G. B., and Doney, S. C.: Changes in Arctic vegetation amplify high-latitude warming through the greenhouse effect, Proceedings of the National Academy of Sciences, 107, 1295-1300, 2010.

Tourre, Y., Jarlan, L., Lacaux, J., Rotela, C., and Lafaye, M.: Spatio-temporal variability of NDVI–precipitation over southernmost South America: possible linkages between climate signals and epidemics, Environmental Research Letters, 3, 044008, 2008.

Wang, G., Hu, H., and Li, T.: The influence of freeze–thaw cycles of active soil layer on surface runoff in a permafrost watershed, Journal of Hydrology, 375, 438-449, 2009.

Wang, K., Zhang, T., and Zhong, X.: Changes in the timing and duration of the near-surface soil freeze/thaw status from 1956 to 2006 across China, The Cryosphere, 9, 1321-1331, 2015.

Willmott, C. J. and Matsuura, K.: Smart interpolation of annually averaged air temperature in the United States, Journal of Applied Meteorology, 34, 2577-2586, 1995.

Willmott, C. J. and Robeson, S. M.: Climatologically aided interpolation (CAI) of terrestrial air

The Cryosphere Discuss., doi:10.5194/tc-2016-129, 2016
Manuscript under review for journal The Cryosphere
Published: 14 July 2016
© Author(s) 2016. CC-BY 3.0 License.

temperature, International Journal of Climatology, 15, 221-229, 1995.

Wu, Q., Hou, Y., Yun, H., and Liu, Y.: Changes in active-layer thickness and near-surface permafrost between 2002 and 2012 in alpine ecosystems, Qinghai–Xizang (Tibet) Plateau, China, Global and Planetary Change, 124, 149-155, 2015.

Wu, Q. and Zhang, T.: Recent permafrost warming on the Qinghai-Tibetan Plateau, Journal of Geophysical Research: Atmospheres, 113, 2008.

Wu, Q., Zhang, T., and Liu, Y.: Permafrost temperatures and thickness on the Qinghai-Tibet Plateau, Global and Planetary Change, 72, 32-38, 2010.

Wu, T., Wang, Q., Zhao, L., Batkhishig, O., and Watanabe, M.: Observed trends in surface freezing/thawing index over the period 1987–2005 in Mongolia, Cold Regions Science and Technology, 69, 105-111, 2011.

Zhang, T.: Influence of the seasonal snow cover on the ground thermal regime: An overview, Reviews of Geophysics, 43, 2005.

Zhang, T., Armstrong, R., and Smith, J.: Investigation of the near-surface soil freeze-thaw cycle in the contiguous United States: Algorithm development and validation, Journal of Geophysical Research: Atmospheres, 108, 2003.

Zhang, T., Barry, R. G., and Armstrong, R. L.: Application of satellite remote sensing techniques to frozen ground studies, Polar Geography, 28, 163-196, 2004.

Zhang, T., Barry, R. G., Knowles, K., Heginbottom, J., and Brown, J.: Statistics and characteristics of permafrost and ground-ice distribution in the Northern Hemisphere 1, Polar Geography, 23, 132-154, 1999.

Zhang, T., Frauenfeld, O. W., Serreze, M. C., Etringer, A., Oelke, C., McCreight, J., Barry, R. G., Gilichinsky, D., Yang, D., and Ye, H.: Spatial and temporal variability in active layer thickness over the Russian Arctic drainage basin, Journal of Geophysical Research: Atmospheres, 110, 2005.

Zhang, T., Osterkamp, T., and Stamnes, K.: Effects of climate on the active layer and permafrost on the North Slope of Alaska, USA, Permafrost and Periglacial Processes, 8, 45-67, 1997.

Zhang, T. and Stamnes, K.: Impact of climatic factors on the active layer and permafrost at Barrow, Alaska, Permafrost and Periglacial Processes, 9, 229-246, 1998.

Zhang, T., Stamnes, K., and Bowling, S.: Impact of the atmospheric thickness on the atmospheric downwelling longwave radiation and snowmelt under clear-sky conditions in the Arctic and Subarctic, Journal of Climate, 14, 920-939, 2001.

Zhang, X.-M., Sheng, Y., Wu, J.-C., Chen, J., Li, J., Cao, Y.-B., and Li, K.: Changes of species diversity indices along the ground temperature of permafrost in the source region of Datong River in the Qilian Mountains, northwestern China, Journal of Beijing Forestry University, 34, 86-93, 2012.

Zhao, L., Ping, C.-L., Yang, D., Cheng, G., Ding, Y., and Liu, S.: Changes of climate and seasonally frozen ground over the past 30 years in Qinghai–Xizang (Tibetan) Plateau, China, Global and Planetary Change, 43, 19-31, 2004.

Zhao, L., Wu, Q., Marchenko, S., and Sharkhuu, N.: Thermal state of permafrost and active layer in Central Asia during the International Polar Year, Permafrost and Periglacial Processes, 21, 198-207, 2010.

Zhong, X., Zhang, T., and Wang, K.: Snow density climatology across the former USSR, The Cryosphere, 8, 785-799, 2014.

The Cryosphere Discuss., doi:10.5194/tc-2016-129, 2016
Manuscript under review for journal The Cryosphere
Published: 14 July 2016
© Author(s) 2016. CC-BY 3.0 License.

Zhou, Y., Guo, D., Qiu, G., and Cheng, G.: Frozen Ground in China, Science Press, Beijing, 450pp, 2000.

© Author(s) 2016. CC-BY 3.0 License.

Figure captions:

Figure 1. The observational station distribution across China, including the 839 air temperature (green dot), 839 ground surface temperature stations (green dot), 845 soil temperature stations (red dot), and elevation. The blue sloid line is the main rivers. The elevation varies between blow 0 m and 8752 m.

Figure 2. Linear least squares regression between soil freeze depth and annual freezing index based on observational sites. The black solid line is the linear fitted line.

Figure 3. Comparison of the simulated and observed SFD for all stations. The red solid line is the 1:1 line; the blue dashed line is regression fit between the simulated and observed values.

Figure 4. Spatial distribution and variability of SFD at the observing stations. (a) Multi-year mean SFD at each site; (b) magnitude of SFD change at each site; (c) the number of sites with different SFD; (d) the number of sites with different SFD changes. The time period of each site is different, mainly controlled by the observation time, but most mainly during 1951-2012.

Figure 5. 1951–2012 SFD anomalies with respect to 30-year baseline (1971-2000) (red solid line) based on up to 839 stations across China as depicted in figure 1. Included also is the 1 standard deviation range (gray shading), the linear trend from 1967 to 2012 (blue dashed line), and 7-year smoothing (green line). The figure in the upper right corner is the observation stations with time series.

Figure 6. Spatial variability of SFD in the decades of the 1950s, 1960s, 1970s, 1980s, 1990s, and 2000s across China.

Figure 7. SFD trends across China from 1950 to 2009. The grey regions mean the SFD change without statistically significant at $p > 0.05$, conversely statistically significant in other regions.

Figure 8. Potential forcing variables of SFD and its trend (black line): (a) red line: mean annual ground surface temperature, (b) green line: mean annual air temperature, (c) cyan line: surface freeze index, (d) magenta line: air freezing index, (e) yellow line: surface thawing index, (f) orange line: air thawing index. All the variables are standardized to range 0–1. R is the correlation coefficient, and all with statistically significant.

Figure 9. Correlation between SFD (top: blue circles) and SND (top: gray circles); Bottom: the number of observing stations contributing to the top time series. The variables are standardized to range 0–1. The negative correlation coefficient between SND and SFD, but without statistically significant.

Figure 10. Correlation between SFD (top: blue circles) and mean annual NDVI (top: gray circles); Bottom: the number of observing stations contributing to the top time series. The variables are standardized to range 0–1. In the upper panel, the negative correlation coefficient R=-0.8 presents there is a strongly significant correlation between NDVI and SFD.

The Cryosphere Discuss., doi:10.5194/tc-2016-129, 2016
Manuscript under review for journal The Cryosphere
Published: 14 July 2016
© Author(s) 2016. CC-BY 3.0 License.

The Cryosphere
Discussions
Open Access

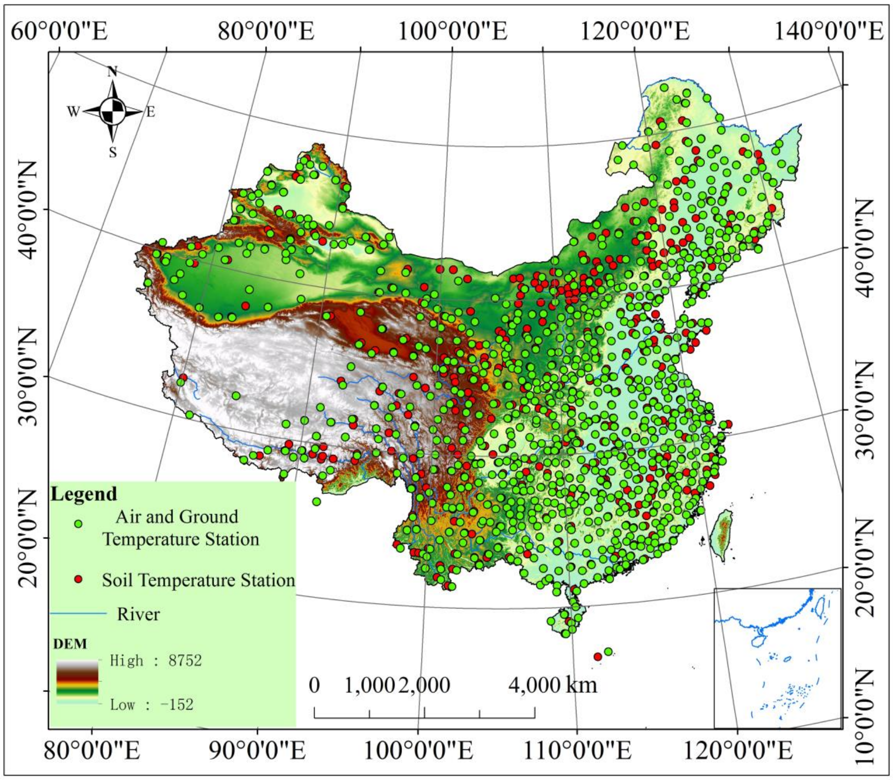

Figure 1. The observational station distribution across China, including the 839 air temperature (green dot), 839 ground surface temperature stations (green dot), 845 soil temperature stations (red dot), and elevation. The blue sloid line is the main rivers. The elevation varies between blow 0 m and 8752 m.

The Cryosphere Discuss., doi:10.5194/tc-2016-129, 2016
Manuscript under review for journal The Cryosphere
Published: 14 July 2016
© Author(s) 2016. CC-BY 3.0 License.

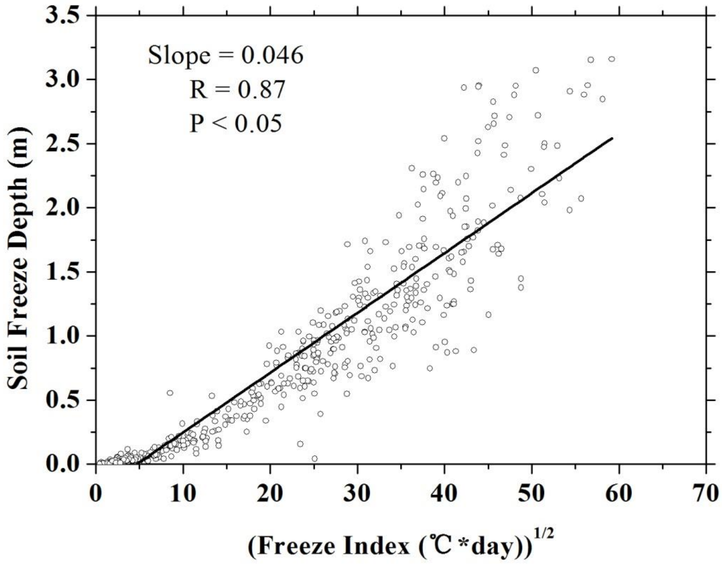

Figure 2. Linear least squares regression between soil freeze depth and annual freezing index based on observational sites. The black solid line is the linear fitted line.

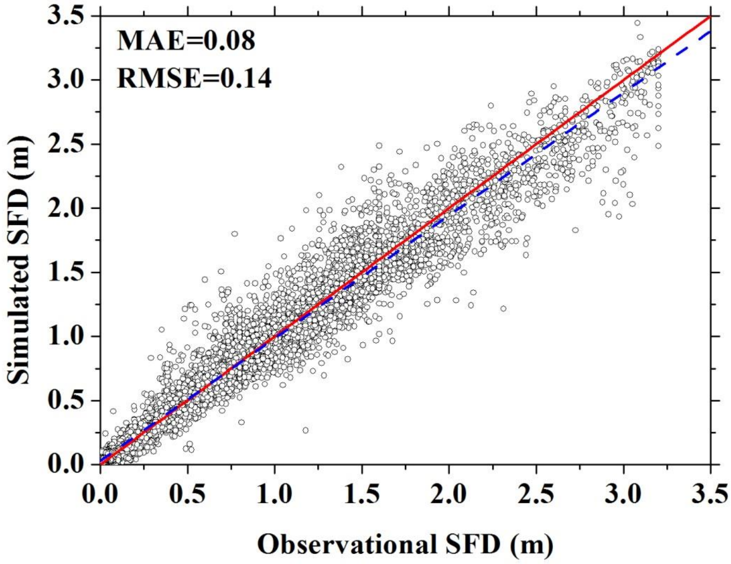

Figure 3. Comparison of the simulated and observed SFD for all stations. The red solid line is the 1:1 line; the blue dashed line is regression fit between the simulated and observed values.

The Cryosphere Discuss., doi:10.5194/tc-2016-129, 2016
Manuscript under review for journal The Cryosphere
Published: 14 July 2016
© Author(s) 2016. CC-BY 3.0 License.

a

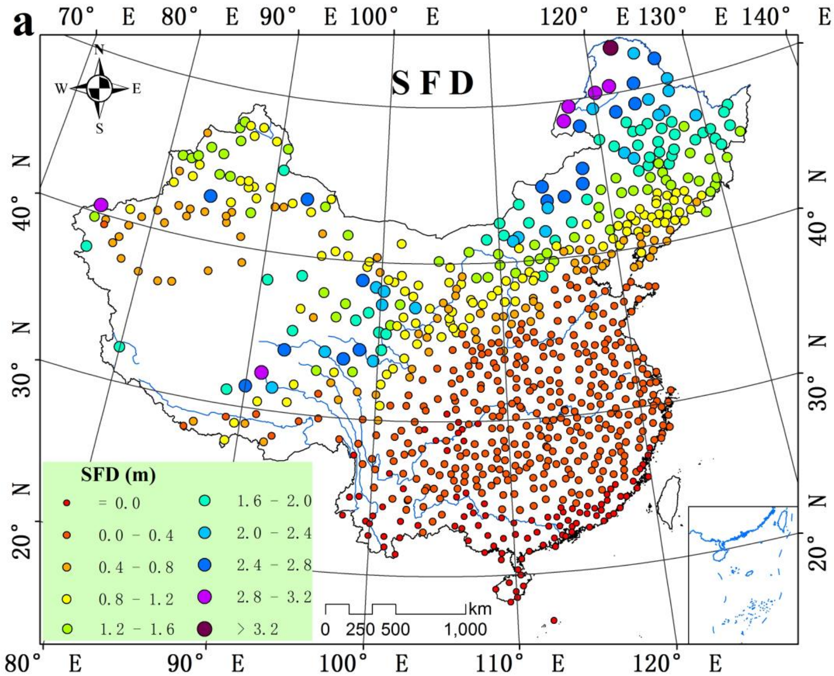

c

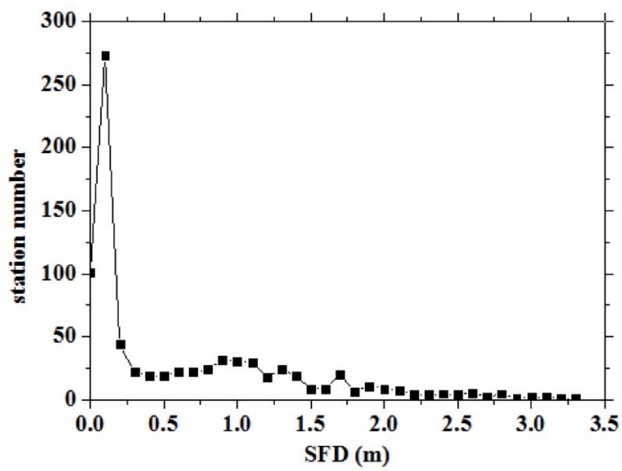

© Author(s) 2016. CC-BY 3.0 License.

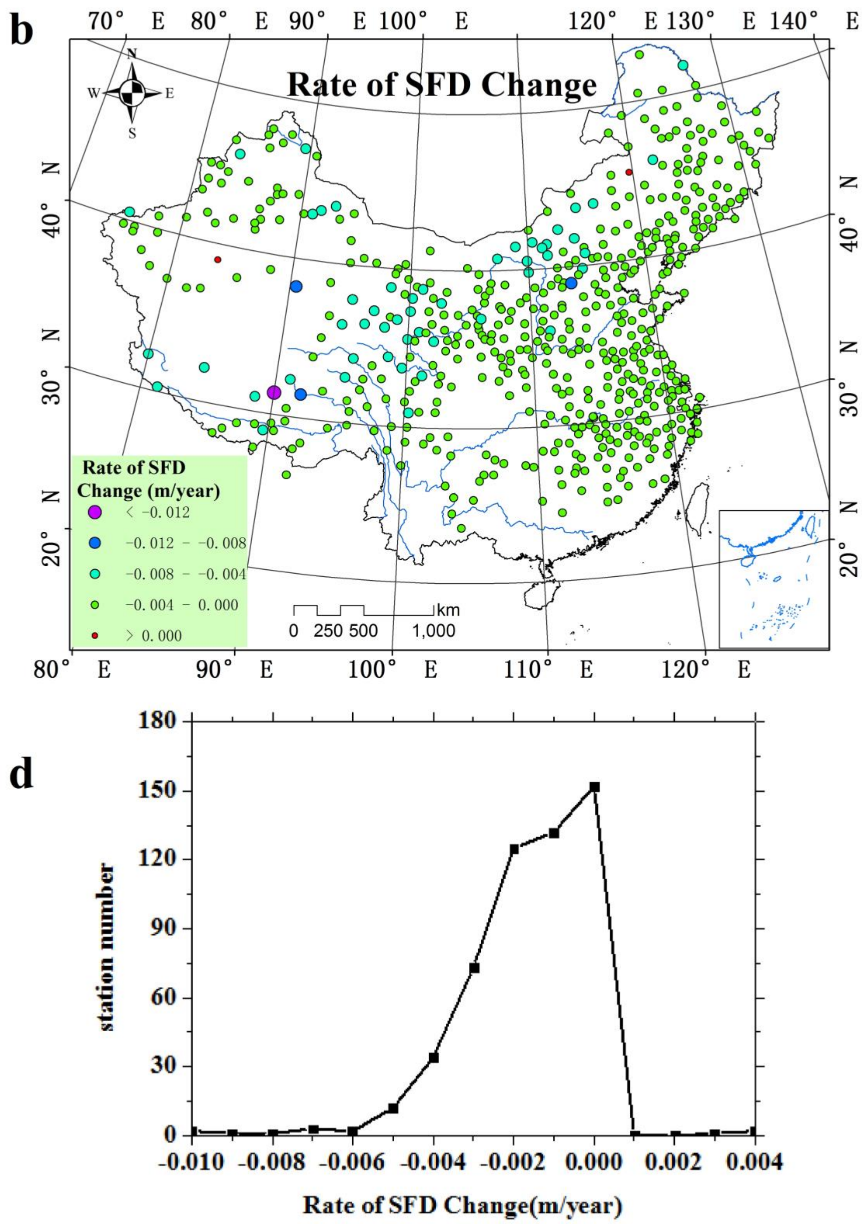

Figure 4. Spatial distribution and variability of SFD at the observing stations. (a) Multi-year mean SFD at each site; (b) magnitude of SFD change at each site; (c) the number of sites with different SFD; (d) the number of sites with different SFD changes. The time period of each site is different, mainly controlled by the observation time, but most mainly during 1951-2012.

The Cryosphere Discuss., doi:10.5194/tc-2016-129, 2016
Manuscript under review for journal The Cryosphere
Published: 14 July 2016
© Author(s) 2016. CC-BY 3.0 License.

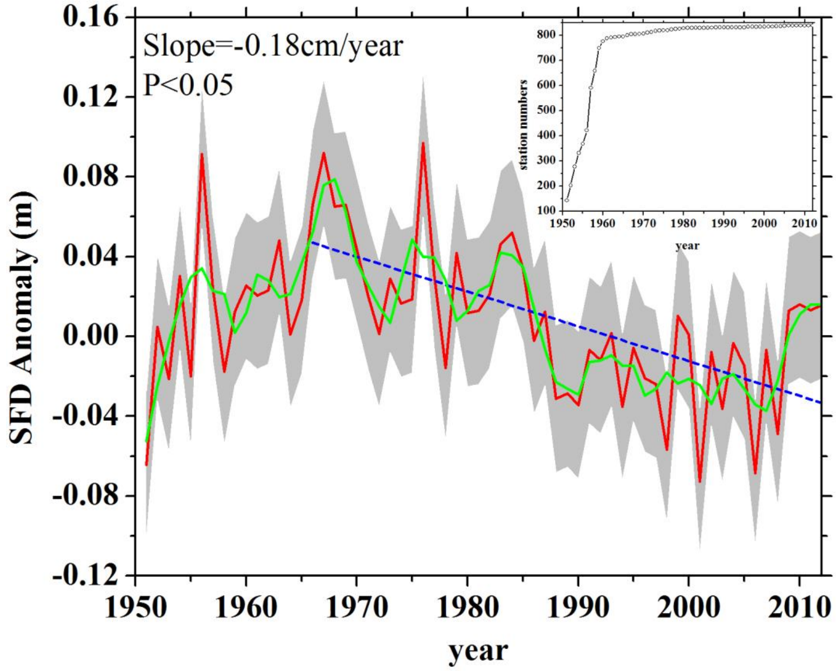

Figure 5. 1951–2012 SFD anomalies with respect to 30-year baseline (1971-2000) (red solid line) based on up to 839 stations across China as depicted in figure 1. Included also is the 1 standard deviation range (gray shading), the linear trend from 1967 to 2012 (blue dashed line), and 7-year smoothing (green line). The figure in the upper right corner is the observation stations with time series.

The Cryosphere Discuss., doi:10.5194/tc-2016-129, 2016
Manuscript under review for journal The Cryosphere
Published: 14 July 2016
© Author(s) 2016. CC-BY 3.0 License.

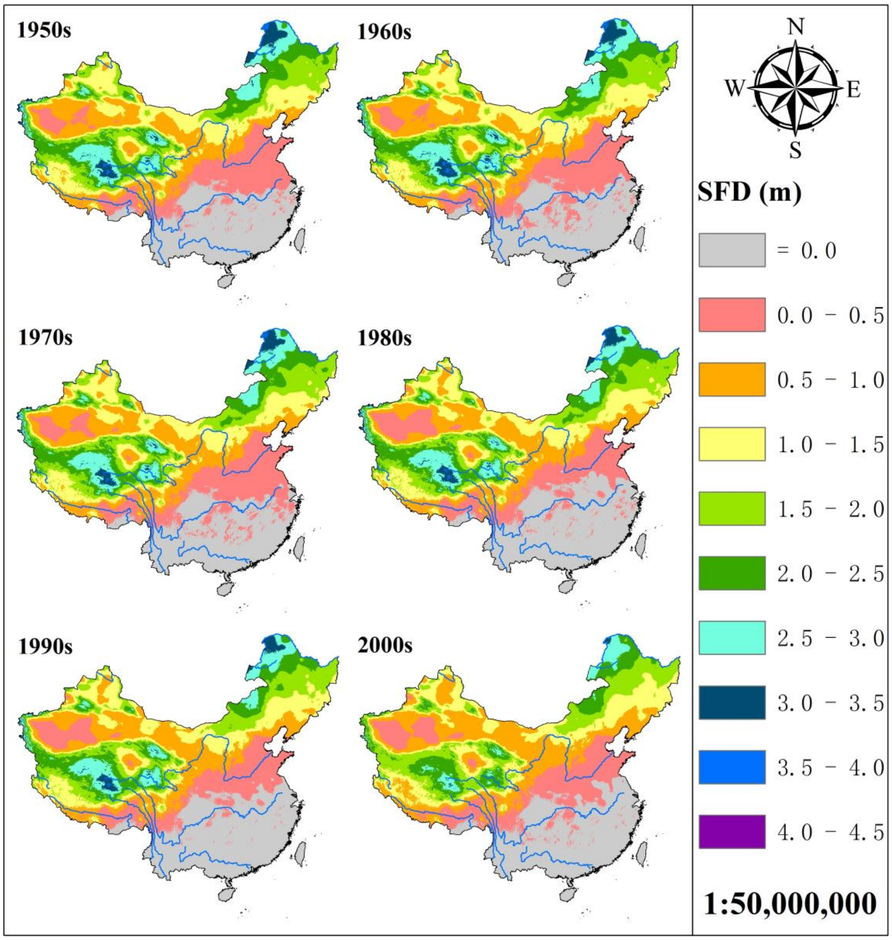

Figure 6. Spatial variability of SFD in the decades of the 1950s, 1960s, 1970s, 1980s, 1990s, and 2000s across China.

© Author(s) 2016. CC-BY 3.0 License.

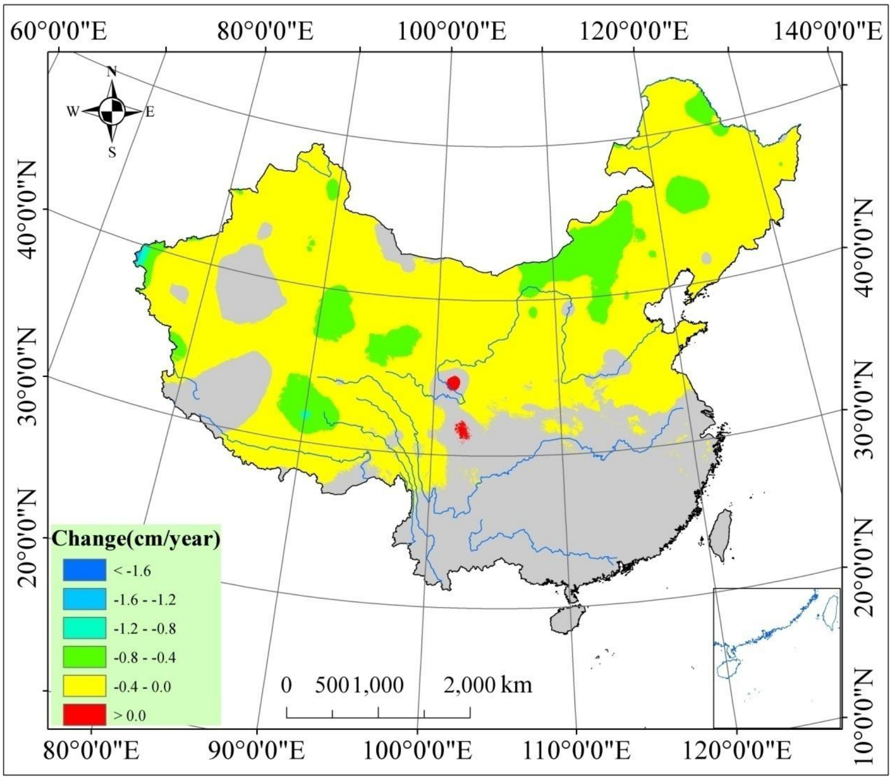

Figure 7. SFD trends across China from 1950 to 2009. The grey regions mean the SFD change without statistically significant at $p > 0.05$, conversely statistically significant in other regions.

The Cryosphere Discuss., doi:10.5194/tc-2016-129, 2016
Manuscript under review for journal The Cryosphere
Published: 14 July 2016
© Author(s) 2016. CC-BY 3.0 License.
The Cryosphere
Discussions
Open Access

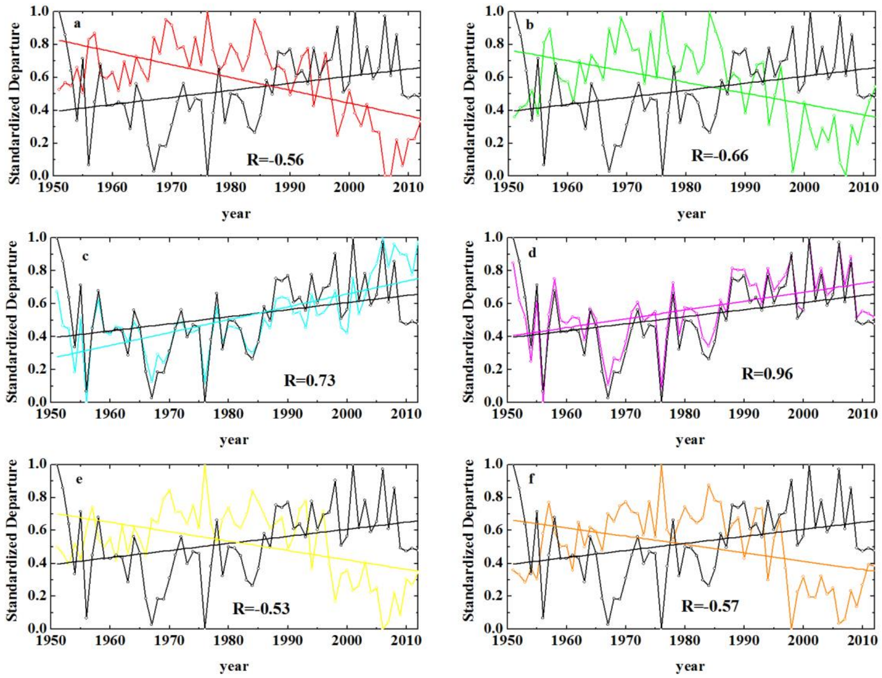

Figure 8. Potential forcing variables of SFD and its trend (black line): (a) red line: mean annual ground surface temperature, (b) green line: mean annual air temperature, (c) cyan line: surface freeze index, (d) magenta line: air freezing index, (e) yellow line: surface thawing index, (f) orange line: air thawing index. All the variables are standardized to range 0–1. R is the correlation coefficient, and all with statistically significant.

The Cryosphere Discuss., doi:10.5194/tc-2016-129, 2016
Manuscript under review for journal The Cryosphere
Published: 14 July 2016
© Author(s) 2016. CC-BY 3.0 License.

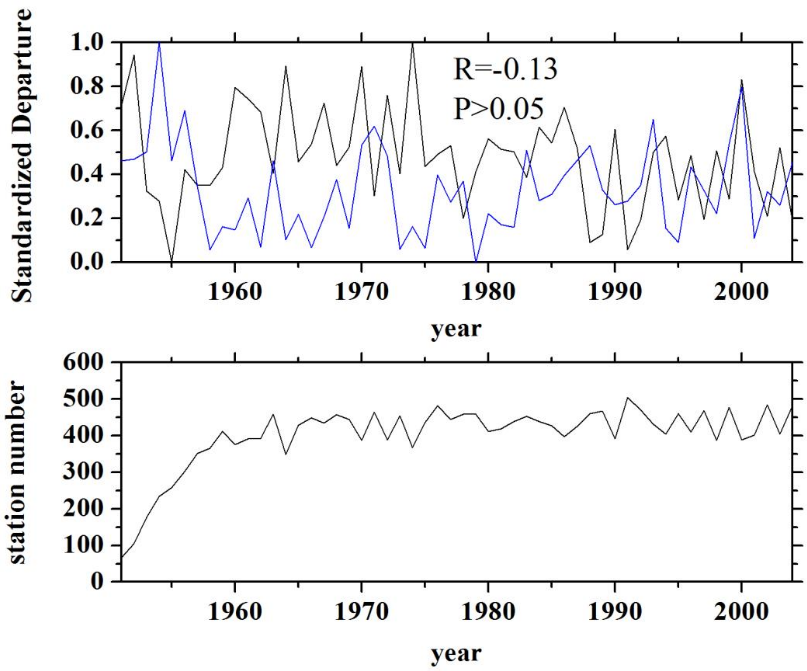

Figure 9. Correlation between SFD (top: blue circles) and SND (top: gray circles); Bottom: the number of observing stations contributing to the top time series. The variables are standardized to range 0–1. The negative correlation coefficient between SND and SFD, but without statistically significant.

© Author(s) 2016. CC-BY 3.0 License.

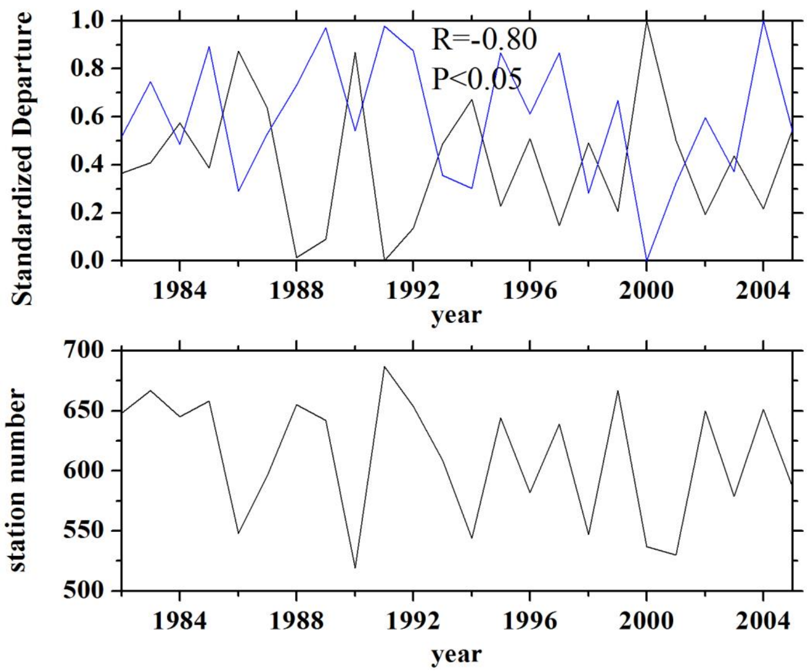

Figure 10. Correlation between SFD (top: blue circles) and mean annual NDVI (top: gray circles); Bottom: the number of observing stations contributing to the top time series. The variables are standardized to range 0–1. In the upper panel, the negative correlation coefficient R=-0.8 presents there is a strongly significant correlation between NDVI and SFD.